Available online at www.sciencedirect.com
ScienceDirect
Mathematics and Computers in Simulation 177 (2020) 603–624
MATHEMATICS AND COMPUTERS IN SIMULATION
www.elsevier.com/locate/matcom

Original articles

In silico study of airway/lung mechanics in normal human breathing

Silvia Marconi[a], Claudio De Lazzari[a,b,*]

[a] Department of Biomedical Science, Institute of Clinical Physiology, C.N.R., Rome 00185, Italy
[b] National Institute for Cardiovascular Research (I.N.R.C.), Bologna 40126, Italy

Received 16 May 2019; received in revised form 5 May 2020; accepted 11 May 2020
Available online 20 May 2020

Abstract

The airway/lung mechanics is usually represented with nonlinear 0-D models based on a pneumatic-electrical analogy.

The aim of this work is to provide a detailed description of the human respiratory mechanics in healthy and diseased conditions. The model used for this purpose employs some known constitutive functions of the main components of the respiratory system. We give a detailed mathematical description of these functions and subsequently derive additional key ones. We are interested not only in the main output such as airflow at the mouth or alveolar pressure and volume, but also in other quantities such as resistance and pressure drop across each element of the system and even recoil and compliance of the chest wall.

Pathological conditions are simulated by altering the parameters of the constitutive functions. Results show that increased upper airway resistance induces airflow reduction with concomitant narrowing of volume and pressure ranges without affecting lung compliance. Instead, increased elastic recoil leads to low volumes and decreased lung compliance.

The model could be used in the study of the interaction between respiratory and cardiovascular systems in pathophysiological conditions.

Keywords: Airway/lung mechanics; Normal human breathing; Nonlinear 0-D model; Numerical simulation; Pleural pressure

1. Introduction

The human respiratory system is a complex network consisting of several components. Mathematical models aim to describe the relationship of the main variables of this system, namely flows, pressures and volumes. 0-D or lumped parameters models based on pneumatic-electrical circuit analogy remain most suitable for this purpose in view of their features where the variables in each compartment are spatially averaged as a function of time.

As initial step towards the development of a complete model of the respiratory system, only the airway/lung mechanics is considered in this work. At present, our aim is to build up a tool for the description of the lung/airway dynamics and investigate its suitability to reproduce the time variation of the main variables.

Once completed and implemented in our numerical virtual patient simulator, this model can be used for study and teaching. In particular, it could be used to evaluate the effects induced by mechanical ventilatory assistance on the hemodynamic and energetic variables of the cardiovascular system.

* Corresponding author at: Department of Biomedical Science, Institute of Clinical Physiology, C.N.R., Rome 00185, Italy.
E-mail address: claudio.delazzari@ifc.cnr.it (C. De Lazzari).

https://doi.org/10.1016/j.matcom.2020.05.014

Many models are available from current literature describing lung/airway mechanics alone [2,3,13,16,23,25,30,33] or the combination of lung/airway mechanics and gas exchange, along with the interaction between the respiratory and the circulatory system [1,15,20–22,26,27,32,38]. These models are all based on the same schematization of the respiratory system and known constitutive functions of the main components such as upper airway and collapsible airway resistances, lung elastic recoil or the transmural pressure. Each of them analyses a particular breathing pattern or breathing manoeuvre, such as panting [16,33], Forced Vital Capacity manoeuvre [26] or Valsalva manoeuvre [21], or focuses on particular aspects of normal breathing, such as the work of breathing [2].

In this work, we use a similar model based on the same structure and the same constitutive functions to give a comprehensive description of the normal breathing pattern and its response under different conditions. For this purpose, we have developed a pleural pressure generator able to reproduce pleural pressure waveforms of quiet breathing close to the real ones. We have selected different normal breathing patterns to analyse the response of the model to different inputs. We are interested not only in the main output such as airflow at the mouth or alveolar pressure and volume, but also in other quantities such as resistance and pressure drop across each element of the system and even recoil and compliance of the chest wall.

We also give a mathematical overview of the constitutive functions of the components used in our model and we derive additional functions, which are not always addressed and graphically represented in studies based on similar models. We focus specifically on the range of the variables related to normal breathing, which ensure the stability of the solution.

Some details on the computational aspects of the study are also provided.

Furthermore, we have tested the behaviour of the model during parameter fluctuation to investigate its ability to reproduce the physiological response of the system to alterations following lung disease. The results of normal breathing simulations are in agreement with the clinical data published in the literature. The alteration of the parameters causes variations in the results consistent with the altered conditions of the system.

2. Methods

2.1. Respiratory system

Current mathematical models of the airway/lung mechanics usually address the component of the respiratory system within the thoracic cavity only, i.e. the lungs and the section of the airways below the larynx. The airways divide into the upper airway, the collapsible airway and the small, or peripheral, airways. The lungs are considered as a unique alveolar region surrounded by the pleural space, containing a limited amount of fluid, which separates it from the chest wall and the diaphragm (Fig. 1). The total lung volume (V_L) is given by [2]:

$$V_L = V_A + V_C + V_D \tag{1}$$

where V_A is the volume of the alveolar region, V_C is the volume of the collapsible airway and V_D is the dead space volume.

The flow of the air at the mouth is the same as the airflow in the upper airway (F). It is considered positive during expiration and negative during inspiration. It is the sum of the flow generated in the alveolar region and in the collapsible airway. The flow rate in these structures is given by the time derivative of the respective volumes ($\dot{V}_A$ and $\dot{V}_C$).

The action of the respiratory muscles and the elastic properties of the lungs generate the necessary pressure to inflate or deflate the lungs. The diaphragm is the main respiratory muscle responsible for inspiration during normal breathing: its movement toward the abdominal cavity causes the downward expansion of the thoracic cavity. Instead, expiration is a passive process: the diaphragm relaxes and the chest wall returns to its resting position due to the elasticity of the chest wall and the lungs, which tend to collapse inward. Nevertheless, during respiratory manoeuvres or exercise, the additional use of intercostal muscles can be required to further expand or contract the rib cage.

The force generated by the muscles and the elastic recoil of the lungs act on the pleural space. When the force of the inspiratory muscles exceeds the lung elastic recoil, the rib cage expands. When muscles relax, the elastic recoil makes the rib cage contract. As a result, in normal breathing the pressure inside the pleural space, that is the pleural or intrathoracic pressure (P_{pl}), remains negative with respect to the environmental pressure (P_{ref}), which is assumed as the reference value and set to zero.

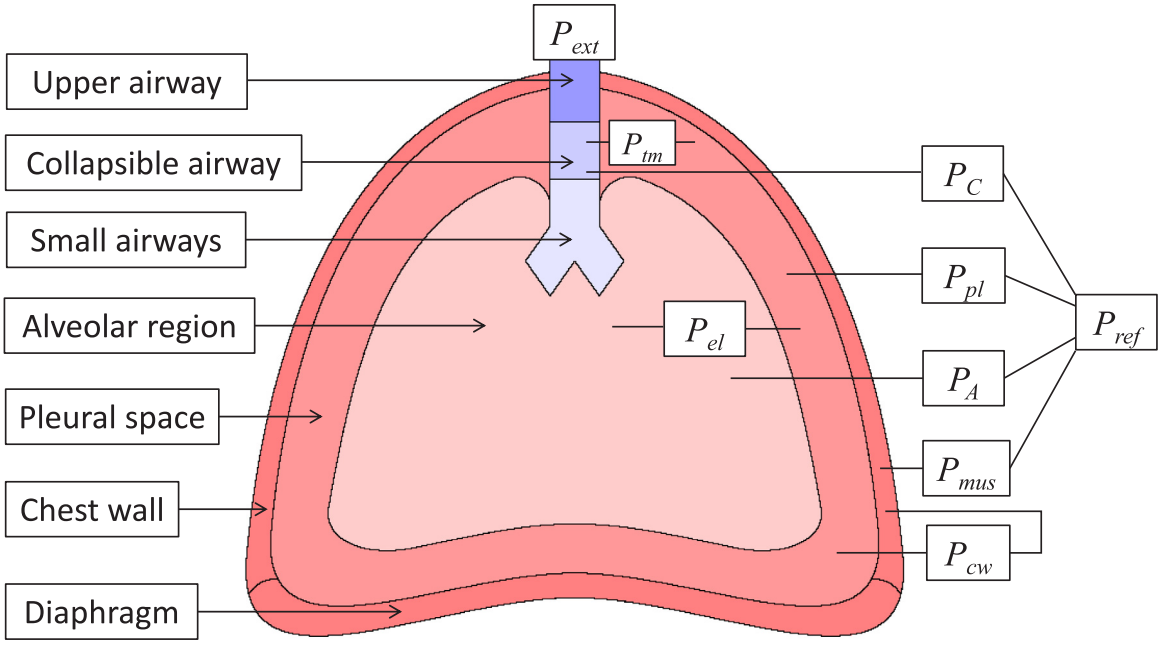

Fig. 1. Schematic representation of the respiratory system and its pressures. The alveolar region is bounded by the pleural space, which separates it from the chest wall and the diaphragm. The alveolar region is connected to the external environment through the airways which divide into the upper airway, the collapsible airway and the small airways. The alveolar pressure P_A, the collapsible pressure P_C, the pleural pressure P_{pl} and the pressure generated by the muscles P_{mus} are referred to the environmental pressure P_{ref}. The transmural pressure P_{tm} is the difference of pressure between the pleural space and the collapsible airway. The elastic recoil of the lung P_{el} is the difference of pressure between the pleural space and the alveolar region. The elastic recoil of the chest wall P_{cw} is the difference of pressure between the pleural space and the chest wall. P_{ext} is the external pressure at mouth. In normal breathing it equals P_{ref}.

The environmental pressure equals the external pressure at the mouth (P_{ext}) during normal breathing. This is not the case during assisted ventilation where the pressure at the mouth is driven by the ventilator [28]. This aspect is not included in this study. Thus, we set:

$$P_{ref} = P_{ext} = 0 \text{ cmH}_2\text{O} \tag{2}$$

The alveolar pressure (P_A), the collapsible airway pressure (P_C) and the pleural pressure (P_{pl}) are referred to the environmental pressure while the dynamic elastic recoil of the lung, or trans-pulmonary pressure (P_{el}), and the transmural pressure (P_{tm}) are referred to P_{pl}:

$$P_A = P_{el} + P_{pl} \qquad P_C = P_{tm} + P_{pl} \tag{3}$$

The pleural pressure is directly related to the action of the muscles: it is the difference between the pressure across the chest wall (P_{cw}) and the pressure generated by the respiratory muscles (P_{mus}) [2]:

$$P_{pl} = P_{cw} - P_{mus} \tag{4}$$

For this reason, we consider the spatially averaged pleural pressure as the driving pressure of the whole system instead of the pressure developed by the muscles: muscle pressure can be derived from pleural pressure and viceversa once the elastic recoil of the chest wall is known. P_{mus} is usually described with a non-realistic sinusoidal function [2,13] whereas P_{pl} is a measurable quantity available from current literature. Therefore, we have aimed to reproduce realistic pleural pressure waveforms and derive P_{mus} from Eq. (4).

2.2. Model description

The electrical circuit that represents the respiratory system consists of four resistances, two capacitors and a generator (Fig. 2). The resistors mimic the airflow resistance of the upper airway (R_U), the collapsible airway (R_C),

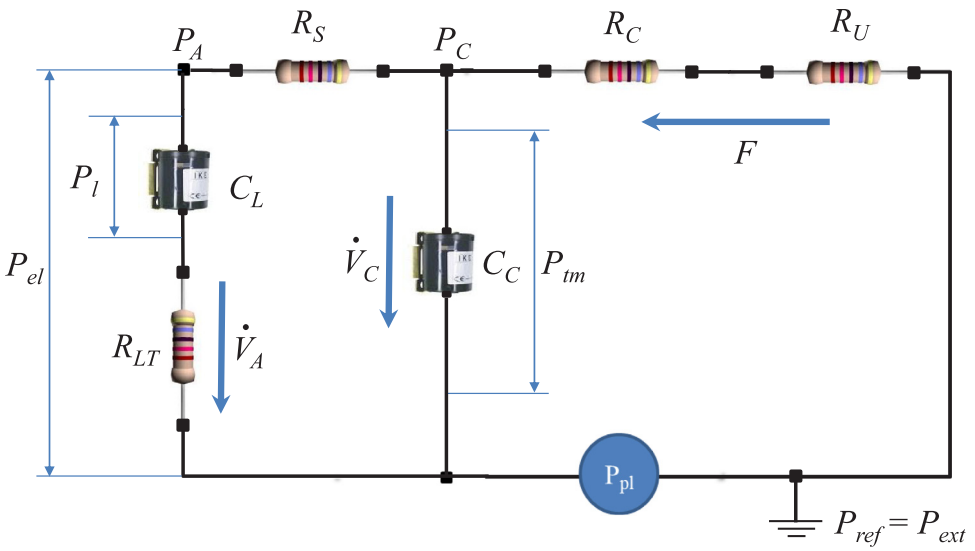

Fig. 2. Electrical analogue of the respiratory system. The four resistors mimic the resistance of the upper airway (R_U), the collapsible airway (R_C), the small airways (R_S) and the lung tissue (R_{LT}) to the airflow. The two capacitors mimic the compliances of the lung (C_L) and of the collapsible airway (C_C). The pressure drop across these elements are the static elastic recoil (P_l) and the transmural pressure (P_{tm}). P_{el} is the dynamic elastic recoil; P_A and P_C are the alveolar and the collapsible pressure, respectively. The generator reproduces the pleural pressure (P_{pl}). The ground corresponds to the environmental reference pressure (P_{ref}). In normal breathing it equals the external pressure at mouth (P_{ext}). The arrows indicate the direction of the airflow (F, $\dot{V}_A$ and $\dot{V}_C$) during inspiration.

the small airways (R_S) and the lung tissue (R_{LT}). The capacitors mimic the compliances of the lung (C_L) and the collapsible airway (C_C). The alternating current generator reproduces the pleural pressure (P_{pl}) that is the pulsatile driving force of the system. The ground corresponds to the environmental reference pressure (P_{ref}) or external pressure at the mouth (P_{ext}) (Eq. (2)) [5,29]. P_{cw} and P_{mus} are not included in the circuit. They would be modelled by replacing the generator of the pleural pressure with a capacitor (with pressure drop P_{cw} and flow $\dot{V}_{cw}$) in series with a generator of muscular pressure linked to the ground.

The parameters of the constitutive functions are patient-dependent. We have used the parameters of a specific patient in [2,26] to plot the graphs of the constitutive functions.

We neglect the time dependence of the variables in the equations.

Upper airway

The upper airway is considered as a rigid tubular structure whose volume is fixed in time and contributes to the dead space volume (V_D). The resistance of the upper airway is usually modelled with a Rohrer resistor [36]:

$$R_U(F) = A_u + K_u \cdot |F| \tag{5}$$

where F ranges between $F_{\min}$ and $F_{\max}$ with $F_{\min} < 0 < F_{\max}$ and A_u and K_u are positive constants. R_U is a linear function of the flow magnitude $|F|$, varying between its minimum value $R_{U\min} = A_u$ at $F = 0$ and maximum value $R_{U\max} = A_u + K_u \cdot F_M$ at the highest flow magnitude $F_M = \max\{|F_{\min}|, F_{\max}\}$. Typically, $|F_{\min}|$ is less than $F_{\max}$ and $F_M = F_{\max}$(Fig. 3[a]). From Ohm's law, the pressure drop (P_{Ru}) is given by:

$$P_{Ru}(F) = R_U(F) \cdot F = A_u \cdot F + K_u \cdot |F| \cdot F \tag{6}$$

At low flow magnitudes the dependence of P_{Ru} on the flow is quite linear, but at high flows the second term ($K_u \cdot |F| \cdot F$) makes it nonlinear (quadratic) (Fig. 3[b]).

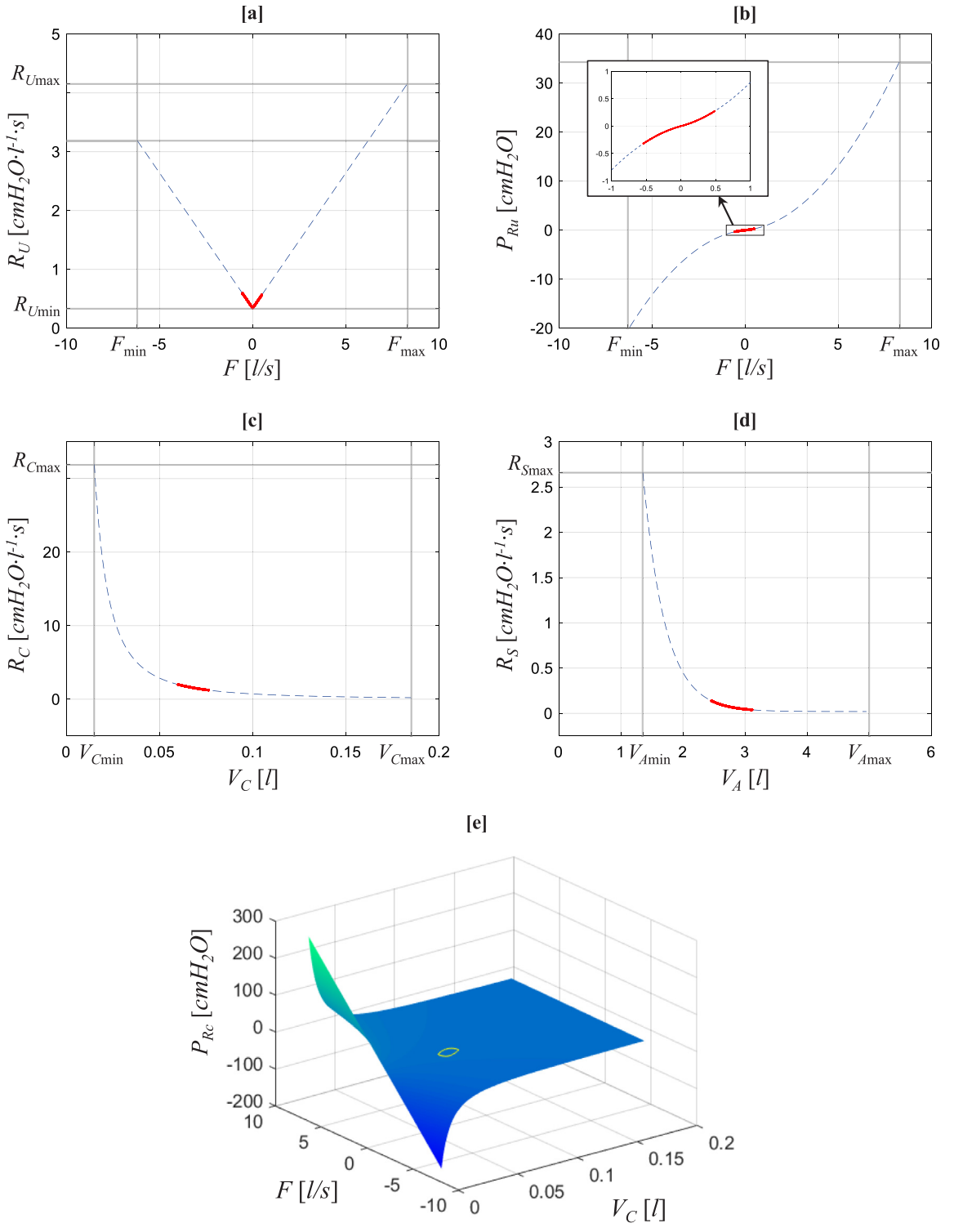

Fig. 3. Resistances and pressures constitutive functions. The continuous thick lines in panels from [a] to [d] and the cycle on the surface in panel [e] correspond to the values obtained during the quiet breathing (i.e. when P^q_{pl} is used as input of the model (see below)). [a] Linear relationship R_U vs F. [b] Quadratic function $P_{Ru}(F)$. The box shows the range of variability of the quiet breathing. [c] and [d] Resistances of the collapsible airway (R_C) and of the small airways (R_S) as functions of the corresponding volumes (V_C and V_A). [e] Pressure drop across the collapsible airway resistance P_{Rc} as function of volume V_C and flow F.

Collapsible airway resistance

The definition of the collapsible airway resistance comes from Poiseuille's law, which expresses the resistance R of a Newtonian fluid of viscosity ρ in laminar flow regime within a cylinder of length L and radius r:

$$R = \frac{8 \cdot \rho \cdot L}{\pi \cdot r^4} \tag{7}$$

Re-writing Eq. (7) in terms of the volume $V = L\pi r^2$ of the cylinder, we obtain:

$$R = \frac{8 \cdot \pi \cdot \rho \cdot L^3}{V^2} \tag{8}$$

Eq. (8) states an inverse proportionality of the resistance to the square of the cylinder volume. If we consider the collapsible airway as a cylinder of fixed length and variable radius, and the air as a viscous Newtonian fluid with laminar flow within it, the above considerations apply. The widely used expression of R_C is [16,33]:

$$R_C\,(V_C) = K_c \cdot \left(\frac{V_{C\,\max}}{V_C}\right)^2 \tag{9}$$

According to Eq. (9), R_C reaches its minimum value $R_{C\min} = K_c$ when the volume of the collapsible airway V_C reaches its maximum value $V_{C\max}$, and its maximum value $R_{C\max} = K_c \cdot (V_{C\max}/V_{C\min})^2$ when V_C reaches its minimum value $V_{C\min}$. It is worth noting that Eq. (9) is not defined at $V_C = 0$ (where the pressure would be infinite), which means that complete airway collapse does not occur (Fig. 3[c]).

The pressure drop (P_{Rc}) is given by (Fig. 3[e]):

$$P_{Rc}\,(V_C, F) = R_C\,(V_C) \cdot F \tag{10}$$

Small airways

The small airways contribute to the model in terms of resistance to the airflow, which is defined as a decreasing exponential function of the alveolar volume [2]:

$$R_S\,(V_A) = A_s \cdot \mathrm{e}^{-K_s \cdot \frac{V_A - V_R}{V^* - V_R}} + B_s \tag{11}$$

where A_s, K_s, B_s and V^* are positive constants and V_R is the residual lung volume at the end of the maximum expiration. R_S reaches its minimum value $R_{S\min}$ when the alveolar volume V_A reaches its maximum value $V_{A\max}$, and its maximum value $R_{S\max}$ when V_A reaches its minimum value $V_{A\min}$ (Fig. 3[d]). Nevertheless, the effect of R_S is significant during a forced expirations whereas it assumes small values during normal breathing. The parameter B_s can be considered constant during normal breathing although it has to be defined as a function of the pleural pressure in the presence of a different breathing pattern or manoeuvre where the pleural pressure becomes positive [26].

Applying Ohm's law, the pressure drop (P_{Rs}) is given by:

$$P_{Rs} = R_S\,(V_A) \cdot \dot{V}_A \tag{12}$$

Lung tissue

The resistance of the lung tissue (R_{LT}), related to its viscous property, is considered constant [26]. Therefore, the pressure drop (P_{Rlt}) is given by:

$$P_{Rlt} = R_{LT} \cdot \dot{V}_A \tag{13}$$

Transmural pressure and collapsible airway compliance

The pressure drop across the two capacitors is defined as a function of the respective volume (Fig. 2).

The transmural pressure is given by the following nonlinear function of V_C [26]:

$$P_{tm}\,(V_C) = \begin{cases} A_c - B_c \cdot \left(D_c - \dfrac{V_C}{V_{C\,\max}}\right)^2 & 0 \le V_C < \dfrac{V_{C\,\max}}{2} \\ A'_c - B'_c \cdot \ln\left(\dfrac{V_{C\,\max}}{V_C} - D'_c\right) & \dfrac{V_{C\,\max}}{2} \le V_C \le V_{C\,\max} \end{cases} \tag{14}$$

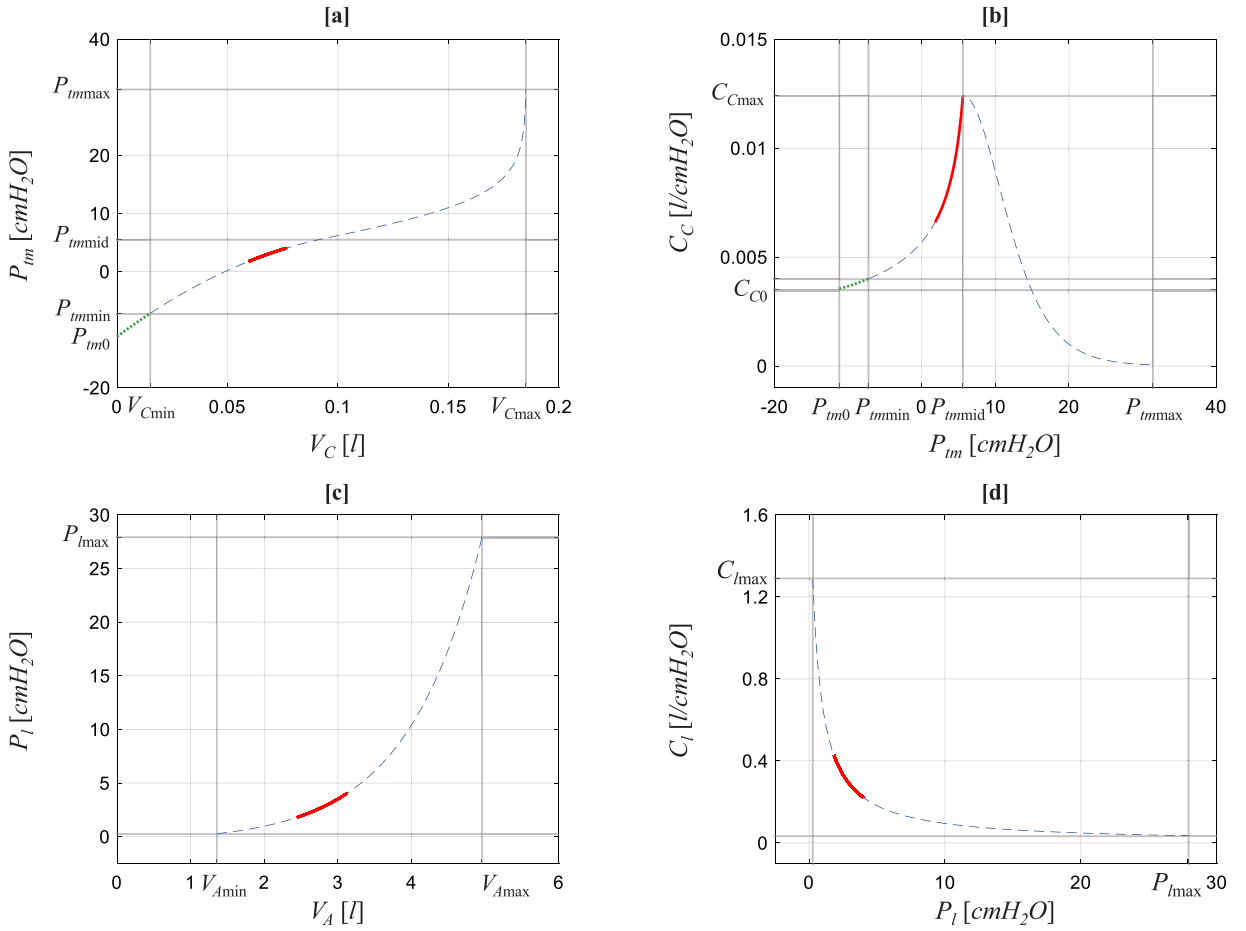

Fig. 4. Transmural pressure, lung elastic recoil and compliances constitutive functions. The continuous thick lines correspond to the values obtained during the quiet breathing (i.e. when P_{pl}^{q} is used as input of the model (see below)). [a] Transmural pressure P_{tm} as function of V_C. The dashed line is the restriction to the interval $[V_{C\min}, V_{C\max}]$. [b] Collapsible airway compliance C_C as function of P_{tm}. The dashed line is the restriction to the interval $[P_{tm\min}, P_{tm\max}]$. [c] Lung elastic recoil P_l as function of V_A. [d] Lung compliance C_l as function of P_l.

where A_c, B_c, D_c, A'_c, B'_c, and D'_c are positive constants. Their values are such that the function is continuous and differentiable at $V_C = V_{C\max}/2$ (Fig. 4[a]). D'_c is a constant value slightly less than 1, which makes P_{tm} positive when V_C reaches $V_{C\max}$, as the argument of the logarithm tends to zero. The expression of the function in Eq. (14) comes from the fact that the inverse function (V_C as function of P_{tm}) must be a sigmoid like function [33]. This is because the volume cannot exceed its maximum and minimum possible values and hence it has small variations at high or low transmural pressures (low compliance). The inverse function of Eq. (14) has the desired sigmoidal shape:

$$V_C\,(P_{tm}) = \begin{cases} V_{C\max} \cdot \left(D_c - \sqrt{\dfrac{A_c - P_{tm}}{B_c}} \right) & P_{tm0} \le P_{tm} < P_{tm\mathrm{mid}} \\ \dfrac{V_{C\max}}{D'_c + e^{-\frac{P_{tm} - A'_c}{B'_c}}} & P_{tm\mathrm{mid}} \le P_{tm} \le P_{tm\max} \end{cases} \tag{15}$$

where $P_{tm0} = A_c - B_c \cdot D_c^2$, $P_{tm\mathrm{mid}} = A'_c - B'_c \cdot \ln(2 - D'_c)$ and $P_{tm\max} = A'_c - B'_c \cdot \ln(1 - D'_c)$ are the values of P_{tm} at $V_C = 0$, $V_C = V_{C\max}/2$ and $V_C = V_{C\max}$ respectively.

Differentiating Eq. (15) with respect to P_{tm}, we obtain the compliance of the collapsible airway:

$$C_C(P_{tm}) = \begin{cases} \dfrac{V_{C\max}}{2\cdot\left[\sqrt{B_c\cdot(A_c - P_{tm})}\right]} & P_{tm0} \le P_{tm} < P_{tm\mathrm{mid}} \\ \dfrac{V_{C\max}\cdot e^{-\frac{P_{tm}-A'_c}{B'_c}}}{B'_c\cdot\left(D'_c + e^{-\frac{P_{tm}-A'_c}{B'_c}}\right)^2} & P_{tm\mathrm{mid}} \le P_{tm} \le P_{tm\max} \end{cases} \tag{16}$$

It reaches its maximum value $C_{C\max} = V_{C\max}\cdot(2 - D'_c)/(4B'_c)$ at $P_{tm} = P_{tm\mathrm{mid}}$ and its minimum values $C_{C0} = V_{C\max}/(2B_c\cdot D_c)$ and $C_{C1} = V_{C\max}\cdot(1-D'_c)/B'_c$ in the left and right intervals at $P_{tm} = P_{tm0}$ and $P_{tm} = P_{tm\max}$ respectively (Fig. 4[b]).

A simplified expression of $V_C(P_{tm})$ is often used [13,25]:

$$V_C(P_{tm}) = \frac{V_{C\max}}{1 + e^{-\frac{P_{tm}-A}{B}}} \tag{17}$$

even if in this case the values 0 and V_{Cmax} must be considered as inferior and superior limits for V_C, since the function in Eq. (17) can never reach those values for any pressure value. On the other hand, we have already seen that Eq. (9) too is not defined at $V_C = 0$. Therefore, it would be more appropriate to consider the interval $[V_{C\min}, V_{C\max}]$ for V_C in Eq. (14). Accordingly, in Eqs. (15) and (16) P_{tm} should be restricted to the interval $[P_{tm\min}, P_{tm\max}]$, where $P_{tm\min} = A_c - B_c\cdot(D_c - V_{C\min}/V_{C\max})^2$ (Fig. 4[a] and [b]). Nevertheless, this is not so relevant when both pressure and volume keep far from their extreme values. Actually, apart from particular breathing manoeuvres, in normal breathing and in most cases, volumes, pressures, resistances and compliances take values in restricted subsets of the intervals discussed so far.

Lung elastic recoil and compliance

The static elastic recoil of the lung is defined as an exponential increasing function of V_A as follows [25]:

$$P_l(V_A) = A_l\cdot e^{K_l\cdot V_A} - B_l \tag{18}$$

where A_l, B_l and K_l are positive constants. Their values are such that $P_l(V_A) + B_l$ remains positive in the variability range of V_A: $[V_{A\min}, V_{A\max}]$ (Fig. 4[c]).

The inverse function of Eq. (18) is:

$$V_A(P_l) = \frac{1}{K_l}\cdot\ln\left(\frac{P_l + B_l}{A_l}\right) \tag{19}$$

Differentiating Eq. (19), we obtain the compliance of the lungs:

$$C_L(P_l) = \frac{1}{K_l\cdot(P_l + B_l)} \tag{20}$$

that is a decreasing function of P_l (Fig. 4[d]).

The dynamic elastic recoil is given by $P_{el} = P_l + P_{Rlt}$.

Considering Eq. (1), the minimum and maximum values of the alveolar and collapsible volumes are such that

$$V_R = V_{A\min} + V_{C\min} + V_D, \qquad TLC = V_{A\max} + V_{C\max} + V_D \tag{21}$$

where TLC is the total lung capacity, defined as the lung volume at the end of the maximum inspiration.

Model statement

Given the previous definitions, we solve the electrical circuit (Fig. 2) according to Kirchhoff's current and voltage laws:

$$\begin{cases} F = \dot{V}_A + \dot{V}_C \\ P_{Ru} + P_{Rc} + P_{tm} + P_{pl} = 0 \\ P_{Rs} + P_l + P_{Rlt} - P_{tm} = 0 \end{cases} \tag{22}$$

We neglect the variables dependence. Solving the system with respect to the volumes, from Eqs. (6), (10), (12) and (13) we obtain:

$$\begin{cases} F = \dot{V}_A + \dot{V}_C \\ R_U \cdot F + R_C \cdot F + P_{tm} + P_{pl} = 0 \\ R_S \cdot \dot{V}_A + P_l + R_{LT} \cdot \dot{V}_A - P_{tm} = 0 \end{cases} \tag{23}$$

Substituting the first equation into the second followed by further rearrangement of the terms, and recalling the constitutive equations of the circuit's elements (Eqs. (5), (9), (11), (14) and (18)), we obtain the complete model:

$$\begin{cases} (R_U + R_C) \cdot \dot{V}_C + (R_U + R_C) \cdot \dot{V}_A + P_{tm} + P_{pl} = 0 \\ (R_S + R_{LT}) \cdot \dot{V}_A + P_l - P_{tm} = 0 \\ R_U = A_u + K_u \cdot |F| \\ R_C = K_c \cdot \left(\dfrac{V_{C\,\max}}{V_C} \right)^2 \\ R_S = A_s \cdot e^{-K_s \cdot \frac{V_A - V_R}{V^* - V_R}} + B_s \\ P_{tm} = \begin{cases} A_c - B_c \cdot \left(\dfrac{V_C}{V_{C\,\max}} - D_c \right)^2 & V_{C\,\min} \le V_C \le \dfrac{V_{C\,\max}}{2} \\ A'_c - B'_c \cdot \ln \left(\dfrac{V_{C\,\max}}{V_C} - D'_c \right) & \dfrac{V_{C\,\max}}{2} < V_C \le V_{C\,\max} \end{cases} \\ P_l = A_l \cdot e^{K_l \cdot V_A} - B_l \end{cases} \tag{24}$$

where P_{pl} is the input of the model.

The governing equations of the above system are nonlinear first order ordinary differential equations. They are solved with respect to the unknowns V_A and V_C over the time interval $[0, T]$ with proper initial conditions:

$$\begin{cases} V_A(0) = V_A^0 \\ V_C(0) = V_C^0 \end{cases} \tag{25}$$

The initial conditions do not affect the steady state solution as long as they remain within the variability range of V_A and V_C.

2.3. Pleural pressure

We consider three different pleural pressure waveforms for the normal breathing pattern: to distinguish them, they will be referred to as regular, quiet and tidal breathing.

The respiratory rate for a healthy adult at rest is 12–18 breaths per minute. For the purposes of our simulations, we have considered a respiratory rate of 12 breaths per minute.

Regular breathing

The pleural pressure for regular breathing is taken from [4]:

$$P_{pl}^r\,(\mathrm{t}) = \begin{cases} a + b \cdot \sin \left(\dfrac{\pi \cdot t}{t_1} \right) & 0 \le t < t_1 \\ a + c \cdot \sin \left(\dfrac{\pi \cdot (t - t_1)}{T_r - t_1} \right) & t_1 \le t \le T_r \end{cases} \tag{26}$$

where T_r is the respiratory period and a, b, c and t_1 are suitable parameters that make the function in Eq. (26) continuous and differentiable (Fig. 5[a]). A vertical offset (*voff*) is added to simulate spontaneous breathing (muscles completely relax after contraction: when muscular pressure is zero, the pleural pressure equals the chest wall pressure).

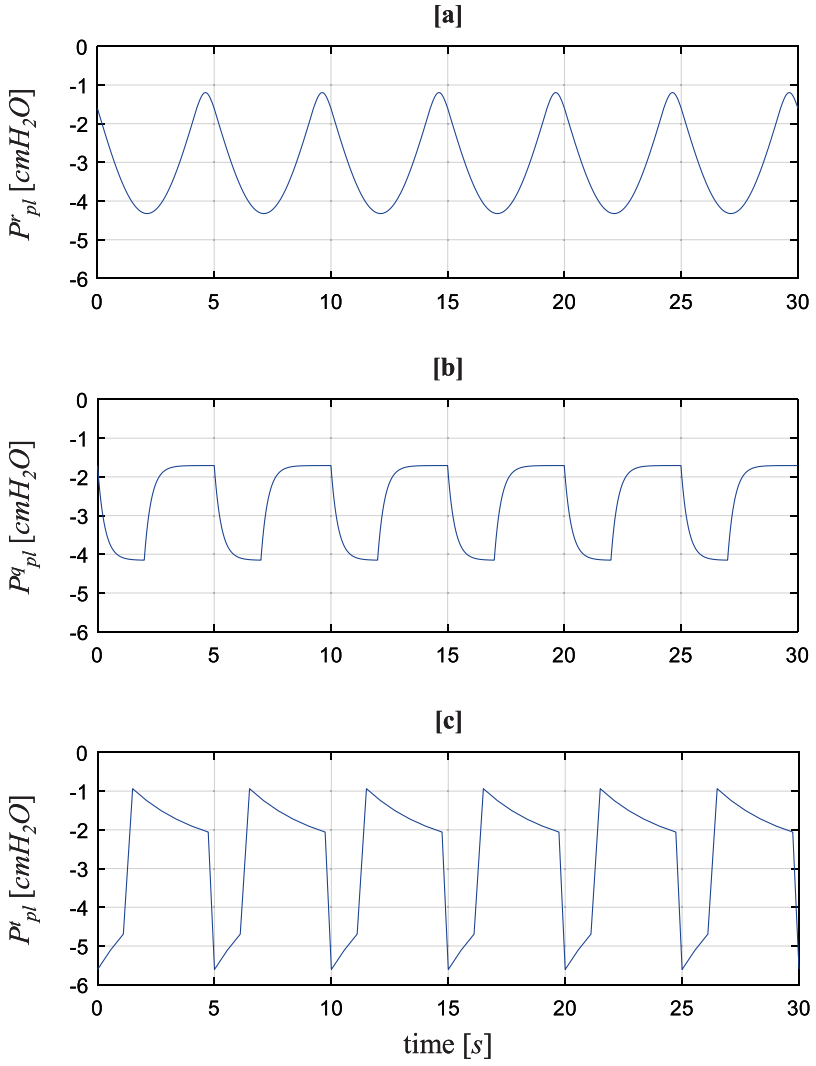

Fig. 5. Examples of pleural pressure waveforms for the normal breathing. [a] Pleural pressure of the regular breathing (P^r_{pl}). [b] Pleural pressure of the quiet breathing (P^q_{pl}). [c] Pleural pressure of the tidal breathing (P^t_{pl}).

Quiet breathing

We developed a pleural pressure generator for quiet breathing by applying a low-pass filter to a pulse generator (Q). In other words, the pulse generator is inserted into a resistor–capacitor (RC) circuit and the pressure drop (P) across the capacitor is considered as the output of the system (Fig. 6, left panel). The circuit is solved according to Kirchhoff's voltage law:

$$R \cdot C \cdot \dot{P} + P = Q \tag{27}$$

where R is the resistance and C is the capacity. The system response can be modified by setting the pulse amplitude (Amp), the duration of the pulse (t_p) in each period (T_r), the phase delay (φ) and the values of R and C. In particular, from Eq. (27) it follows that the solution P depends on the product $R \cdot C$. So we can keep C constant and vary R. A gain (g) and a vertical offset ($voff$) can be applied in order to obtain the desired final pleural pressure waveform (P^q_{pl}), like the one in Fig. 5[b], as previously published [1,27].

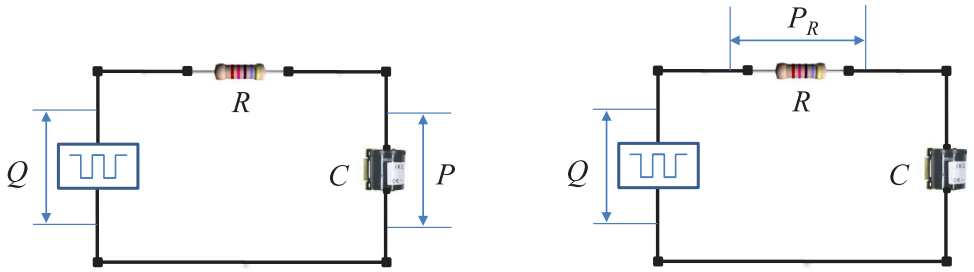

Fig. 6. Filters. Low pass (left panel) and high pass (right panel) filter of a pulse generator (Q). R and C are the resistance and the capacity of the circuit. The pressure drop across the capacitor (P) is the output of the low pass filter. The pressure drop across the resistor (P_R) is the output of the high pass filter.

Tidal breathing

The pleural pressure waveform of tidal breathing is obtained by applying a high-pass filter to a pulse generator (Q). Again, the pulse generator is inserted into the same RC circuit related to quiet breathing but the pressure drop (P_R) across the resistor is considered as the output of the system (Fig. 6, right panel):

$$P_R = Q - P \tag{28}$$

where P is the solution of Eq. (27). Again, the parameters can be set to obtain the desired final pleural pressure waveform (P^t_{pl}), like the one in Fig. 5[c] as previously published [30].

2.4. Combined lung–chest wall system

The chest wall is a compliant system with volume $V_{cw} = V_A + V_C$.

The pressure across the chest wall is a function of the volume with a sigmoidal shape: it is high negative at low volumes (the chest wall tends to expand) and becomes positive at high volumes (the chest wall tends to collapse) (Fig. 7[a]). It is given by the function [2]:

$$P_{cw}(V_{cw}) = A_{cw} - B_{cw} \cdot \ln\left(\frac{TLC - V_R}{V_{cw} - V_R} - D_{cw}\right) \tag{29}$$

where A_{cw} and B_{cw} are suitable positive constants. D_{cw} is a constant slightly less than 1, which makes P_{cw} positive when V_{cw} tends to TLC as the argument of the logarithm tends to zero.

The derivative of the inverse function $V_{cw}(P_{cw})$ is the compliance of the chest wall (C_{cw}):

$$V_{cw}(P_{cw}) = \frac{TLC - V_R}{e^{\frac{A_{cw} - P_{cw}}{B_{cw}}} + D_{cw}} + V_R \tag{30}$$

$$C_{cw}(P_{cw}) = \frac{(TLC - V_R) \cdot e^{\frac{A_{cw} - P_{cw}}{B_{cw}}}}{B_{cw} \cdot \left(e^{\frac{A_{cw} - P_{cw}}{B_{cw}}} + D_{cw}\right)^2} \tag{31}$$

Both the elastic recoil of the chest wall (P_{cw}) and the elastic recoil of the lungs (P_l) act on the pleural space. Combining them, we obtain the elastic recoil of the respiratory system (P_{syst}) (Fig. 7[a]):

$$P_{syst} = P_l + P_{cw} \tag{32}$$

The combined system is in its resting position at the end of a normal breath, when the two opposite elastic recoils balance ($P_{cw} = -P_l$); in this case the lung volume is the functional residual capacity. The system expands at lower volumes and collapses at higher volumes. At volumes higher than the resting volume of the chest wall, both P_{cw} and P_l are positive causing the chest wall and the lungs to collapse (Fig. 7[a]). The slope of the pressure–volume curves is the compliance of the corresponding element. The chest wall and the lungs show similar compliance within the range of normal breathing. The compliance of the combined system is always less than the two compliances alone (Fig. 7[b]).

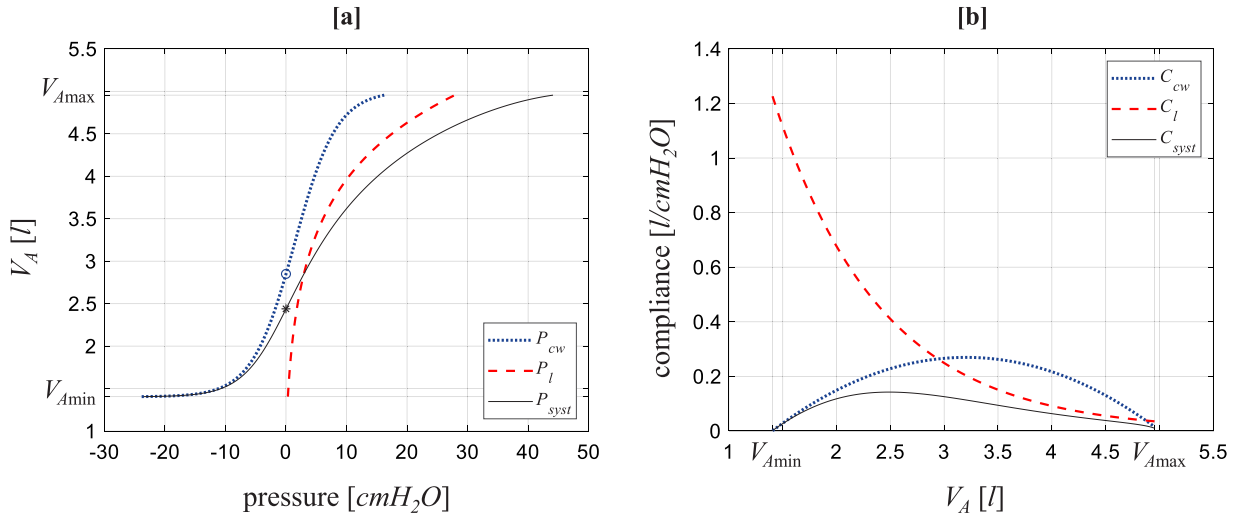

Fig. 7. Pressure–alveolar volume and compliances curves for the considered subject. [a] P_{cw} (dotted line), P_l (dashed line), P_{syst} (continuous line). The star denotes the resting position of the combined lung–chest wall system. The circle denotes the resting position of the chest wall alone. [b] C_{cw} (dotted line), C_l (dashed line), C_{syst} (continuous line) vs alveolar volume.

Table 1 gives a summary of the symbols of the variables and quantities of the respiratory system with their description and measurement units.

2.5. System perturbation

Some of the features of the respiratory system can be altered in particular conditions [4,17,18,24,39,40]. If the airways resistance is increased, breathing becomes more difficult: less air enters and exits the lung, resulting in reduced maximum and increased minimum lung volumes. The contribution of the small airways to the overall resistance is lower because, even if they have small sections, air distribution occurs over a wide number of branches. Instead, the upper and collapsible airways resistance depends on their size (Eq. (7)). Obstructive lung disease such as asthma and chronic obstructive pulmonary disease cause increasing resistance due to airways obstruction.

Lung disease can even affect the elastic properties of lung tissue with alteration of lung compliance. If the elastic recoil of the lung is decreased by a loss of elastic fibres, it is easier for the chest wall to move and spring out. The wider chest wall movement causes greater volume variations with increased compliance. These are the features of emphysematous disease. Conversely, if the elastic recoil of the lung is increased because of increased stiffness of the lung tissue, it is harder for the chest wall to expand. The restricted chest wall movement causes lower volume variations with decreased compliance. These are the features of restrictive lung disease with particular reference to pulmonary fibrosis. The deficiency of surfactant in the alveoli can also reduce lung compliance as observed in neonatal respiratory distress syndrome.

A diseased status of the respiratory system can be simulated by modifying the parameters of the constitutive functions describing the resistances and the elastic recoil.

2.6. Model implementation

The model has been implemented in MATLAB and solved in the Simulink environment [37]. Simulink is a powerful tool to solve and analyse initial condition problems for linear and nonlinear ordinary differential equations. The dynamic system equations are graphically represented by means of blocks connected through suitable links. Fig. 8 shows the Simulink block diagram solving the model equations (Eq. (24)). Each block contains the instructions that define the corresponding element. The block "P_{pl}" contains the instructions to create the input pleural pressure, for example the pleural pressure for regular, quiet and tidal breathing. Fig. 9 shows the Simulink block diagrams which solve the RC circuit (Eq. (27)) and generate the pleural pressure for quiet and tidal breathing.

Table 1
Symbols, their description and unit.

Symbol	Description	Unit
C_C	Collapsible airway compliance	l/cmH_2O
C_{cw}	Chest wall compliance	l/cmH_2O
C_L	Lung compliance	l/cmH_2O
C_{syst}	Compliance of the lung-chest wall system	l/cmH_2O
F	Airflow at the mouth	l/s
P_A	Alveolar pressure	cmH_2O
P_C	Collapsible airway pressure	cmH_2O
P_{cw}	Chest wall pressure	cmH_2O
P_{el}	Dynamic lung elastic recoil	cmH_2O
P_{ext}	Pressure at mouth	cmH_2O
P_l	Static lung elastic recoil	cmH_2O
P_{mus}	Muscular pressure	cmH_2O
P_{pl}	Pleural pressure	cmH_2O
P_{ref}	Environmental pressure	cmH_2O
P_{syst}	Elastic recoil of the lung-chest wall system	cmH_2O
P_{tm}	Transmural pressure	cmH_2O
R_C	Collapsible airway resistance	cm$H_2O \cdot l^{-1} \cdot s$
R_{LT}	Lung tissue resistance	cm$H_2O \cdot l^{-1} \cdot s$
R_S	Small airways resistance	cm$H_2O \cdot l^{-1} \cdot s$
R_U	Upper airway resistance	cm$H_2O \cdot l^{-1} \cdot s$
TLC	Total lung capacity	l
V_A	Alveolar space volume	l
V_C	Collapsible airway volume	l
V_{cw}	Chest wall volume	l
V_D	Dead space volume	l
V_L	Total lung volume	l
V_R	Residual volume	l

Many numerical schemes with fixed or variable time step are available in Simulink to solve the differential problems. We solved the model with a variable time step using Dormand–Prince method with relative tolerance 1×10^{-6}.

Table 2 lists all model parameters used in the simulations. The parameters for the pleural pressures are available in Table 3.

3. Results

The range of oscillation of the resistances and their pressure drops, the compliances, the transmural pressure and the lung elastic recoil obtained with the model have been already shown in Figs. 4 and 5 for quiet breathing, i.e. applying P_{pl}^q as input of the model. Similar ranges are obtained with regular breathing although the time waveforms are quite different due to the different shape of the input pleural pressures (Fig. 10).

The same applies to the airflow (Fig. 11[a] and [b]), the alveolar volume (Fig. 11[c] and [d]) and the flow–volume and flow–pressure loops (Fig. 11[e], [f], [g] and [h]). The flow–volume loop is counterclockwise (Fig. 11[e] and [f]). The lung volume is referred to the residual volume. In normal breathing, the difference $V_L - V_R$ remains positive because the lungs never collapse to the residual volume. The collapsible volume has the same waveform of the corresponding alveolar volume, but varies within a much smaller range ([0.0606 ÷ 0.0775 l] in regular breathing and [0.0600 ÷ 0.0764 l] in quiet breathing, not shown). All these curves are specific for each mode of breathing.

Both the pleural pressures of regular and quiet breathing have been derived to obtain a normal breathing pattern: at the end of expiration (and at the beginning of inspiration), muscles are completely relaxed ($P_{mus} = 0$). From Eq. (32), this means that the pleural pressure and the chest wall pressure are equal (Fig. 12[a] and [b]). The static and the elastic recoil of the lung are slightly different due to the resistance of lung tissue, which causes hysteresis of the dynamic elastic recoil of the lung. In Fig. 12[a], they are represented in a Campbell diagram (they are reversed in the pressure–volume plane) [6]. The pleural pressure exhibits hysteresis too (Fig. 12[a]). This is due to the surface tension of the liquid lining the alveoli, which opposes a greater resistance to inflation than deflation.

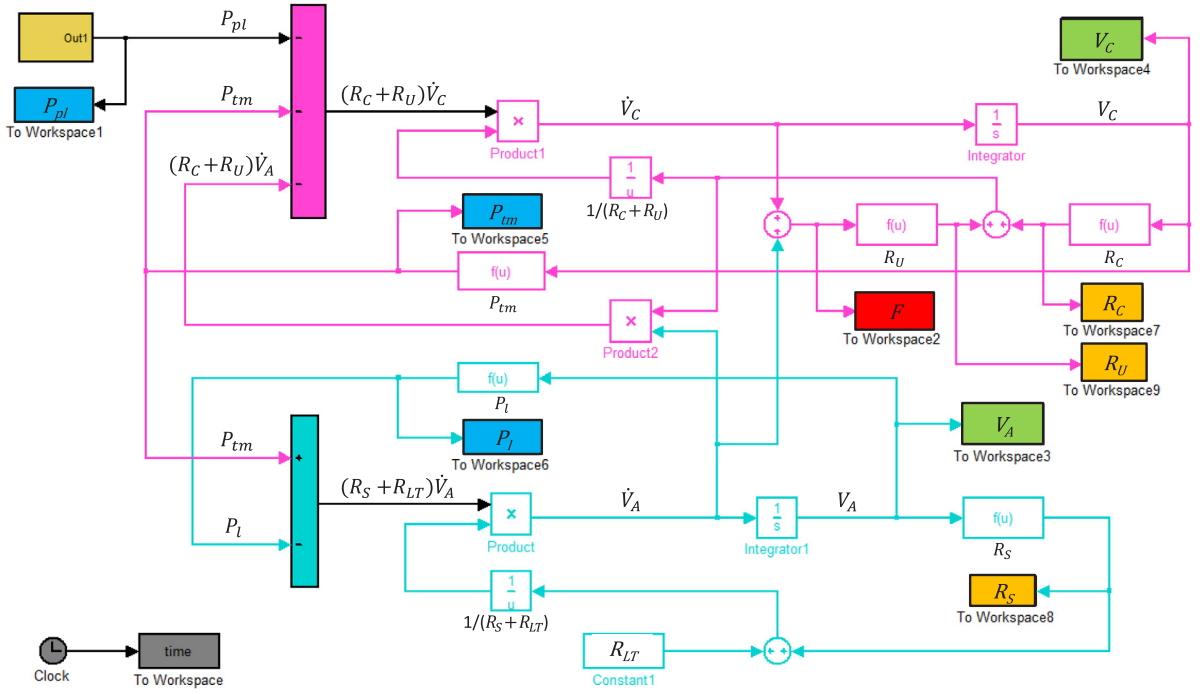

Fig. 8. Simulink block diagram of the model. The top left box defines the pleural pressure that is the input of the model. The vertical rectangles represent the first two equations in Eq. (24), that are linked through the transmural pressure P_{tm} and the flow in the alveolar region $\dot{V}_A$.

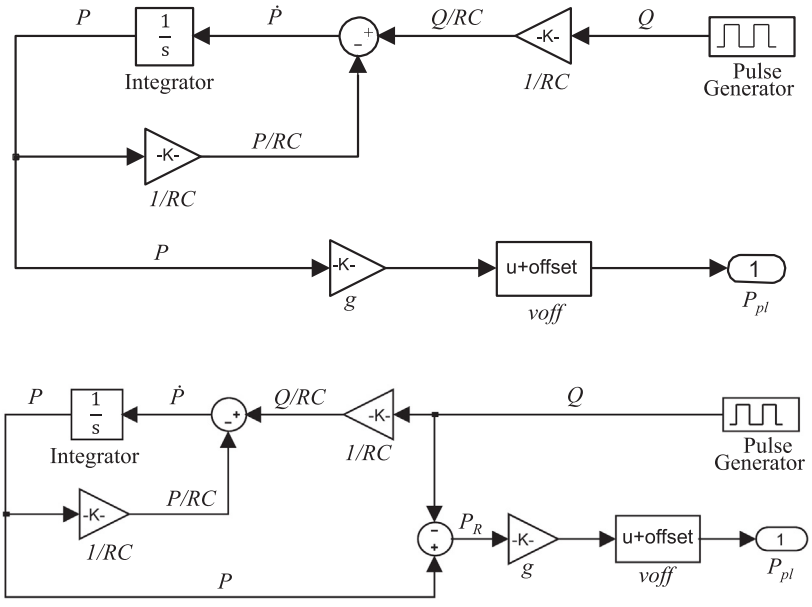

Fig. 9. Simulink block diagrams of the pleural pressure generators. The upper block solves Eq. (27) and generates the pleural pressure of the quiet breathing by applying a gain g and a vertical offset *voff* to the output P. The lower block solves Eqs. (27) and (28) and generates the pleural pressure of the tidal breathing by applying a gain g and a vertical offset *voff* to the output P_R.

If the parameters of the model are modified, the system response to the same pleural pressure changes: the solution of the system converges to a different steady state, resulting in volume, pressure and flow variation

Table 2
Parameters of the model [2,26].

Parameter	Value	Unit
A_c (A'_c)	7.09 (5.6)	cmH_2O
A_{cw}	1.4	cmH_2O
A_l	0.2	cmH_2O
A_s	2.2	$cmH_2O \cdot l^{-1} \cdot s$
A_u	0.34	$cmH_2O \cdot l^{-1} \cdot s$
B_c (B'_c)	37.3 (3.73)	cmH_2O
B_{cw}	3.5	cmH_2O
B_l	0.5	cmH_2O
B_s	0.02	$cmH_2O \cdot l^{-1} \cdot s$
D_c (D'_c)	0.7 (0.999)	
D_{cw}	0.999	
$F_{\min}$ ($F_{\max}$)	−6.2 (8.3)	l/s
K_l	1.00	
K_s	10.9	
K_u	0.46	$cmH_2O \cdot l^{-2} \cdot s^2$
K_c	0.21	$cmH_2O \cdot l^{-1} \cdot s$
R_{LT}	0.2	$cmH_2O \cdot l^{-1} \cdot s$
TLC	5.19	l
V^*	5.3	l
V_A^0 (V_C^0)	2.2 (0.05)	l
$V_{C\min}$ ($V_{C\max}$)	0.015 (0.185)	l
V_D	0.05	l
V_R	1.42	l

Table 3
Parameters of the pleural pressures.

Parameter	Value		Unit
	P^r_{pl}		
a	–4.0785		cmH_2O
b	–2.719		cmH_2O
c	0.40785		cmH_2O
T_r	5		s
t_1	$0.85 \cdot T_r = 4.25$		s
$voff$	2.474		cmH_2O
	P^q_{pl}	P^t_{pl}	
C	1	2	$l \cdot cmH_2O^{-1}$
R	0.3	3	$cmH_2O \cdot l^{-1} \cdot s$
Amp	1	−4	cmH_2O
t_p	2	1.5	s
T_r	5	5	s
φ	0	0	s
g	−2.4471	1	
$voff$	−1.7075	–2.635	cmH_2O

compared to baseline conditions. We have changed the value of a single parameter in each experiment. We show the results for quiet breathing.

We have changed the parameters of the constitutive functions of the resistances: A_u, K_u, K_c, A_s, K_s and B_s. Fig. 13 shows the results of the simulations performed by changing the parameter K_u related to the upper airways resistance. Similar results have been obtained varying the other parameters (not shown). In all cases we have observed that an increasing resistance causes narrowing of flow and volume ranges (Fig. 13[a], [b] and [c]) and widening of the alveolar pressure range (Fig. 13[d]) without affecting compliance (Fig. 13[e]).

Fig. 14 shows the results of the simulations performed by changing the parameter K_l that is related to the elastic recoil of the lung. Similar results have been obtained varying the parameters A_l and B_l (not shown). In all cases

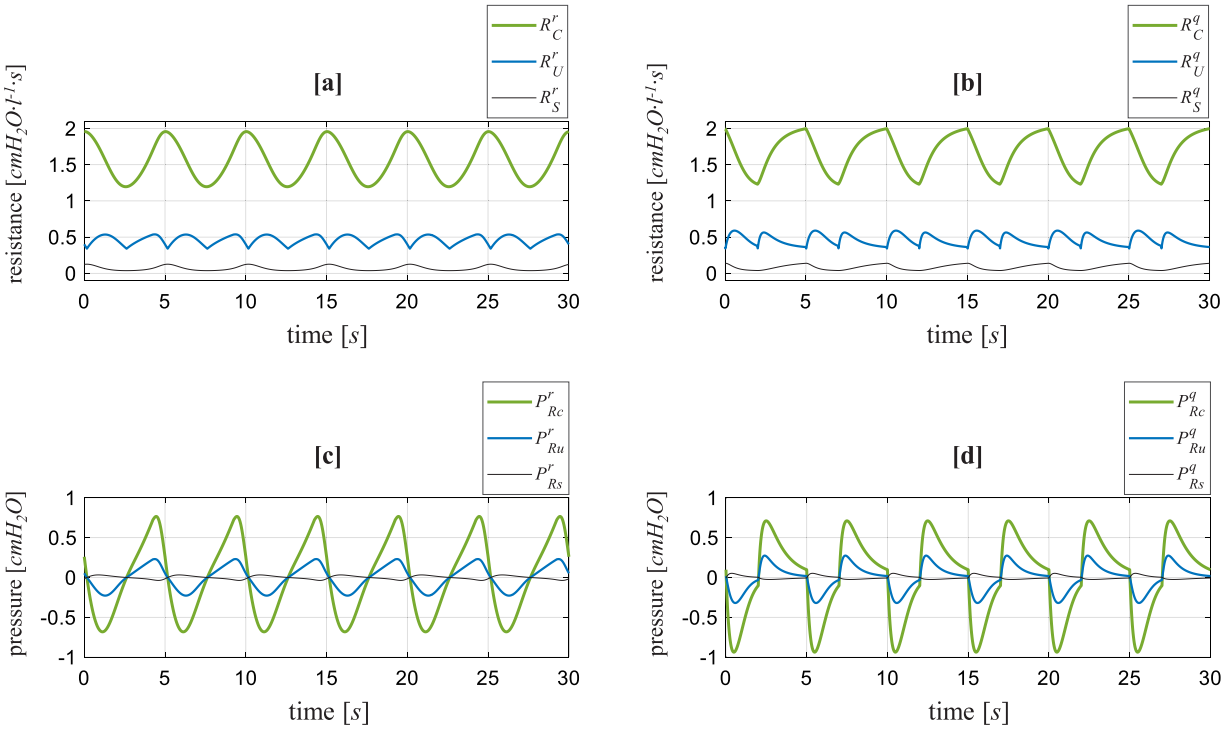

Fig. 10. Regular and quiet breathing. Time variations of resistances and pressures when P^r_{pl} (regular breathing - left) and P^q_{pl} (quiet breathing - right) are applied as input of the model. [a] and [b] R^r_C and R^q_C (thick line), R^r_U and R^q_U (normal line) R^r_S and R^q_S (thin line). [c] and [d] P^r_{Rc} and P^q_{Rc} (thick line), P^r_{Ru} and P^q_{Ru} (normal line) P^r_{Rs} and P^q_{Rs} (thin line).

we have observed that an increasing elastic recoil causes not only narrowing of flow and volume ranges, but also shifting of the volume towards low values (Fig. 14[a], [b] and [c]) as well as narrowing of the alveolar pressure range (Fig. 14[d]) with concomitant decrease in lung compliance (Fig. 14[e]). All graphs obtained from the simulations show the results once the solution has reached the steady state.

4. Discussion

The lack of patho-physiological clinical data made us consider data measured by other research groups [2,26] to validate our model. Our results are in agreement with the values relative to normal breathing reported in [2,21,26].

Measured values in diseased conditions are not available in the cited works, because they consider only specific manoeuvres. Our aim is to show that the same model can be used to describe altered conditions of the system, at least in a qualitative way [8,14,19]. According to Eqs. (1) and (21), the total lung volume cannot go below the residual volume and cannot exceed the total lung capacity. Consequently, the total lung volume referred to the residual volume must range between 0 and the upper limit $V_{Amax} + V_{Cmax} - V_{Amin} - V_{Cmin}$. The amount of modifications of the parameters K_u and K_l takes these limitations into account. In particular, we have made sure that the total lung volume did not reach the extremes. In fact, extreme values can be reached during particular breathing manoeuvres, such as FVC, but not in normal breathing, due to expiratory (ERV) and inspiratory (IRV) reserve volumes: $IRV = TLC - \max(V_A) - \max(V_C)$, $ERV = \min(V_A) + \min(V_C) - V_R$.

In addition, the values of the parameters must ensure the convergence of the solution to a steady state. The baseline value of K_u is close to 0 $\mathrm{cmH_2O \cdot l^{-2} \cdot s^2}$. The system becomes unstable when K_u is about 30 $\mathrm{cmH_2O \cdot l^{-2} \cdot s^2}$. We set the values of K_u much less than that threshold, making sure that the volume excursion (tidal volume), that is the amount of air moved during each breath, remained physiologically acceptable. The outcome of our simulations gave 7.6% and 13.2% reduction in tidal volume compared to baseline.

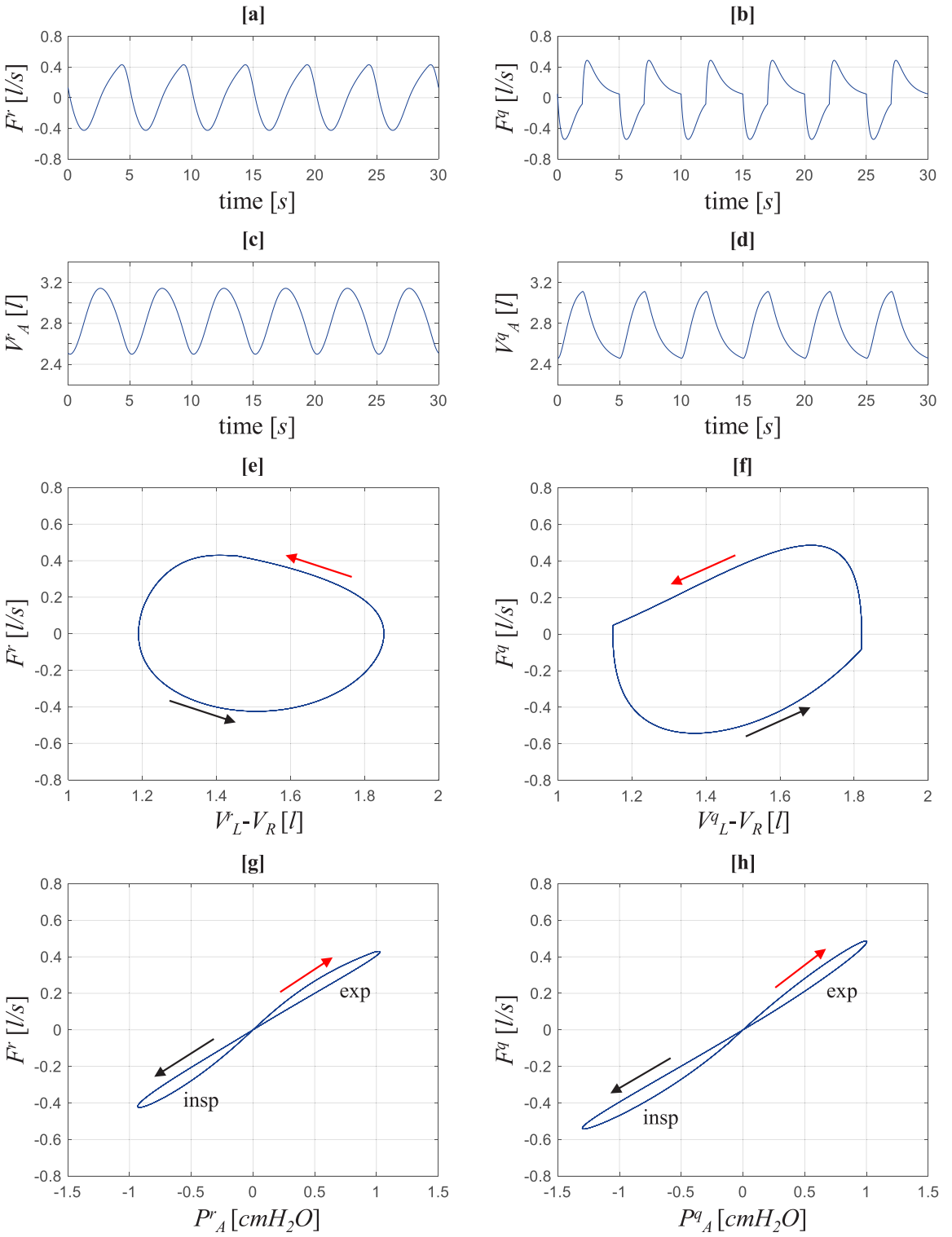

Fig. 11. Regular and quiet breathing. Results of the simulations when P^r_{pl} (regular breathing - left) and P^q_{pl} (quiet breathing - right) are applied as input of the model. [a] and [b] Airflow at the mouth. [c] and [d] Alveolar volume. [e] and [f] Flow–volume loops (total lung volume referred to the residual volume). The loop is counterclockwise. [g] and [h] Flow–alveolar pressure loop. Flow and alveolar pressures are simultaneously negative during inspiration (insp) and positive during expiration (exp).

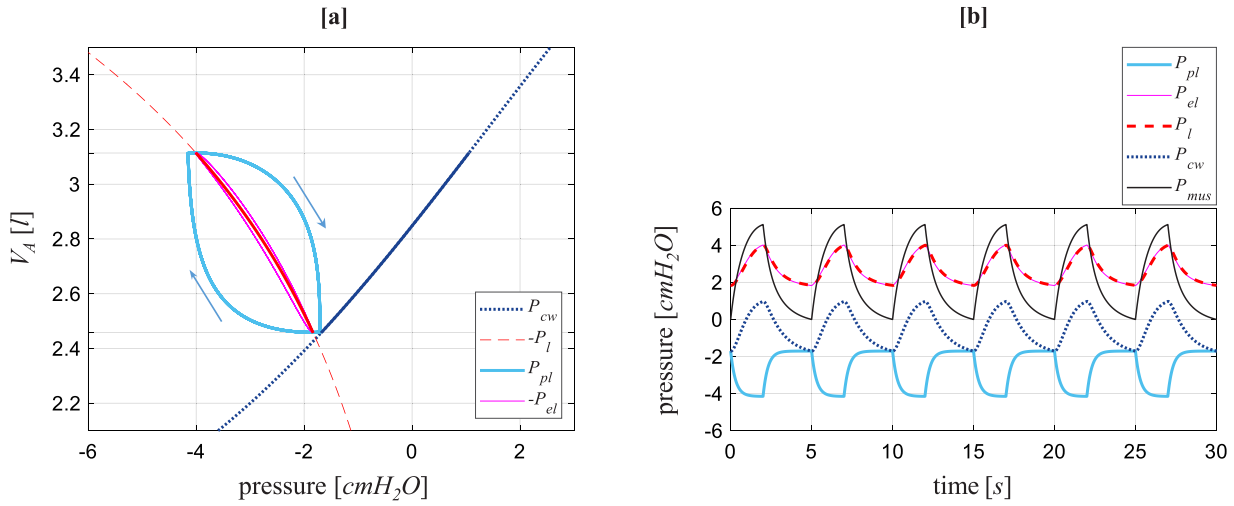

Fig. 12. Pressures in quiet breathing. [a] Campbell pressure–volume diagram: chest wall recoil (dotted line), reversed static (dashed line) and dynamic (thin continuous loop around -P_l) lung elastic recoil, pleural pressure (thick loop) and alveolar pressure (thin loop) vs alveolar volume (V_A). The thick lines indicate the oscillations in quiet breathing. [b] Time variation of the pressures: chest wall recoil (dotted line), static and dynamic lung elastic recoils (dashed and thin continuous juxtaposed lines), pleural pressure (thick line) and muscular pressure (normal dark line).

We made similar considerations to set K_l: in order to ensure the limitations of the total lung volume discussed above, K_l must range between 0.6 and 1.8. The solution is stable for all cases. The outcome of our simulations gave 21.3% reduction and 31.4% increase in mean total lung volume compared to baseline.

Bearing in mind that both TLC and V_R may vary under a diseased status compared to baseline [31], the outcome of our simulations remains reliable when both parameters are kept constant. The amount of *TLC* and V_R variation from the healthy status due to obstructive or restrictive lung diseases is not available in current literature and we have not measured data of these quantities. Therefore, measured data for these quantities could not be used to define a relationship between the variation of the parameters and the corresponding variation of *TLC* and V_R.

The model presented in this work has been intentionally kept simple because we are mainly interested in the description of normal breathing. It does not account for airways turbulence, which is absent in normal breathing. A different relationship between the flow and the upper airway resistance should be defined in this case [34,35]. Furthermore, we model the viscoelastic properties of lung tissue with a single resistance. Finally, we have not considered the possibility for the small airways resistance to depend on pleural pressure.

5. Conclusions

Mathematical modelling and simulation of the respiratory system may have a role to play for the evaluation of the respiratory function and may be a useful approach for the diagnosis, treatment and prognosis of various respiratory disorders.

The nonlinear lumped parameter model of the airway/lung mechanics presented in this work describes the time variation and the relationship of the main variables of the respiratory system during normal breathing in healthy and pathological conditions.

The results of normal breathing simulations are in agreement with the clinical data published in the literature. The alteration of the parameters causes variations in the results consistent with the altered conditions of the system.

Further studies are being considered to address other aspects of the respiratory system including other breathing patterns and gas exchanges. The features of our respiratory model may well be suitable to interact with our numerical virtual patient simulator CARDIOSIM© [9,10,12]. The novelty is a 0-D model of the respiratory system with the ability to interact with a software like CARDIOSIM©, which has already shown its potential for clinical application [7,9] and teaching purposes [10,11]. The implementation of this respiratory model in CARDIOSIM© may be useful to study the interaction between the cardiovascular and respiratory system during cardiac assistance [9].

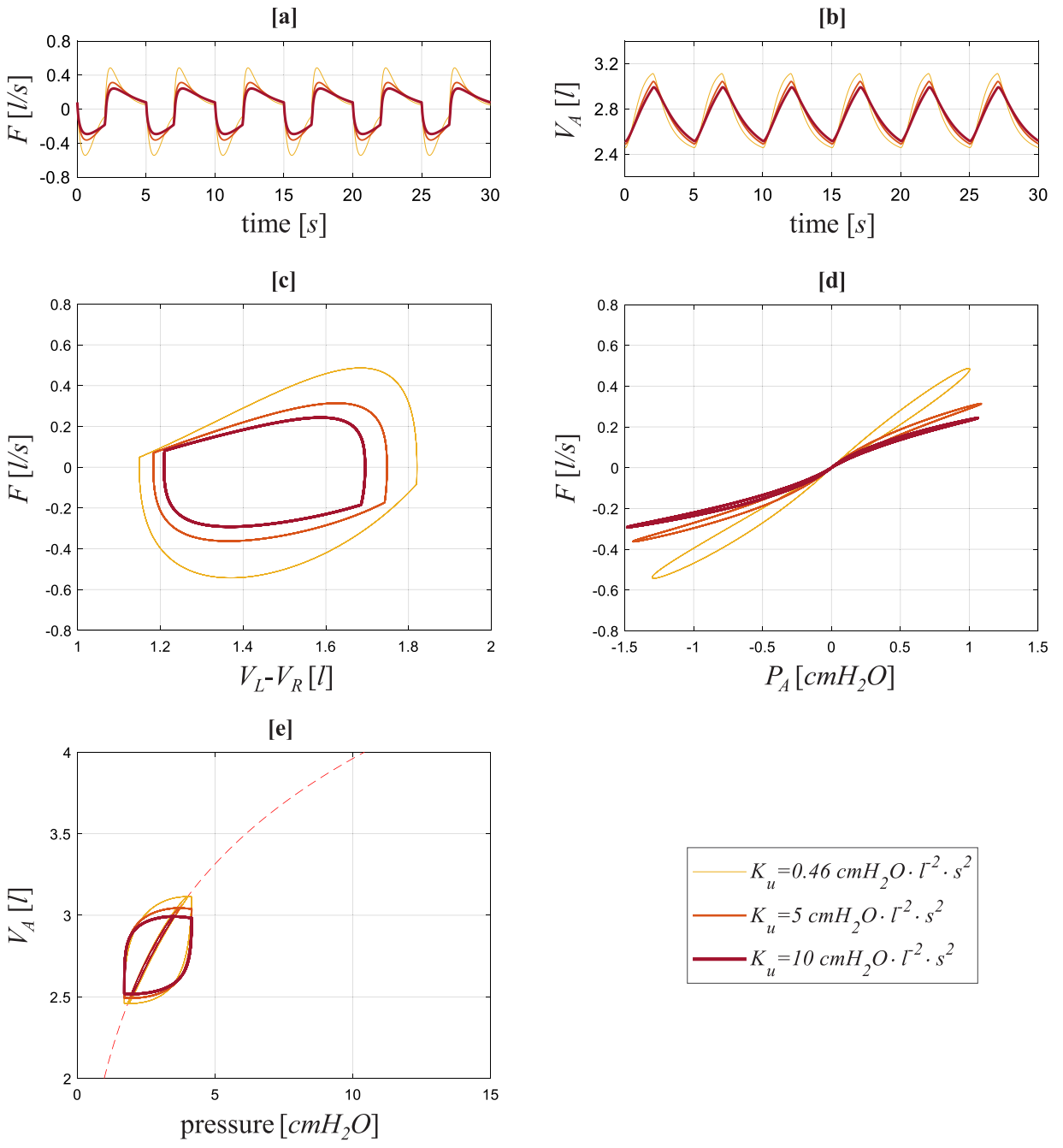

Fig. 13. Results of the simulations for the quiet breathing changing the parameter K_u. [a] Airflow at the mouth. [b] Alveolar volume. [c] Flow–volume loop (total lung volume referred to the residual volume). The loop is counterclockwise. [d] Flow–alveolar pressure loop. [e] Static (dashed line) and dynamic (thin continuous loop around P_l) lung elastic recoil and reversed pleural pressure (external loop) vs alveolar volume. All panels show the results obtained with $K_u = 0.46$ $\mathrm{cmH_2O \cdot l^{-2} \cdot s^2}$ that is the base value (thin line), $K_u = 5$ $\mathrm{cmH_2O \cdot l^{-2} \cdot s^2}$ (normal line) and $K_u = 10$ $\mathrm{cmH_2O \cdot l^{-2} \cdot s^2}$ (thick line).

Once the model presented in this work is completed and inserted into CARDIOSIM©, it can be used in clinical environment to evaluate the effects induced by mechanical ventilatory assistance on the hemodynamic and energetic variables of the cardiovascular system. These studies are useful, for example, to understand how

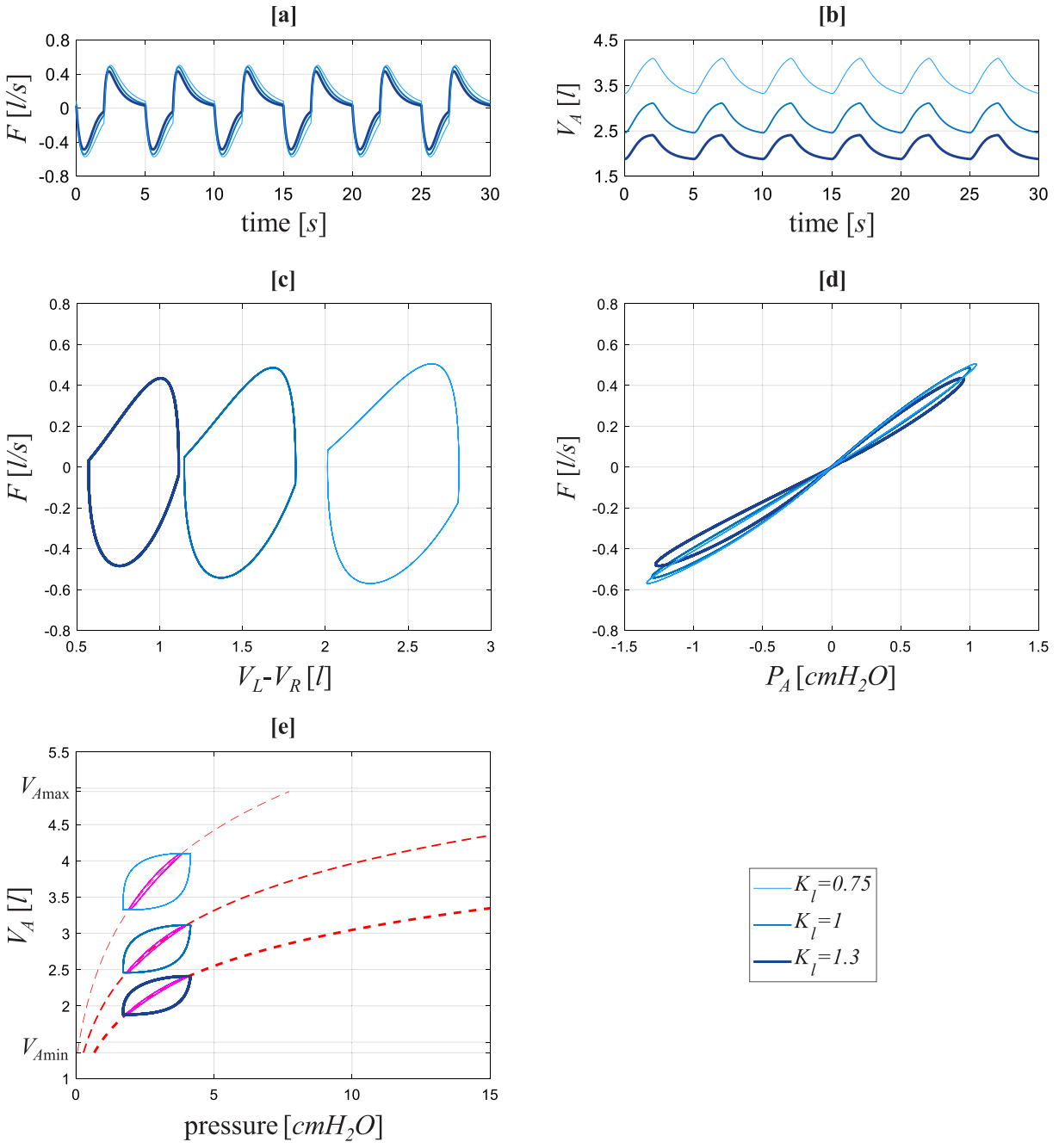

Fig. 14. Results of the simulations for the quiet breathing changing the parameter K_l. [a] Airflow at the mouth. [b] Alveolar volume. [c] Flow–volume loop (total lung volume referred to the residual volume). The loop is counterclockwise. [d] Flow–alveolar pressure loop. [e] Static (dashed line) and dynamic (thin continuous loop around P_l) lung elastic recoil and reversed pleural pressure (external loop) vs alveolar volume. All panels show the results obtained with $K_l = 0.75$ (thin lines), $K_l = 1$ that is the base value (normal line) and $K_l = 1.3$ (thick line).

to manage mechanical ventilation in ventilated COVID-19 patients. The experience gained during the COVID-19 pandemic has shown that the management of mechanical ventilation assistance in presence of extracorporeal

membrane oxygenation (ECMO) or intra-aortic balloon pump (IABP) is critical and changes from patient to patient depending on the side diseases afflicting the patient. The numerical simulator can be a useful tool to help medical doctors in the best management of devices that improve the patient's conditions.

Declaration of competing interest

The authors declare that they have no known competing financial interests or personal relationships that could have appeared to influence the work reported in this paper.

Acknowledgements

This work was supported by the Italian Ministry of Education, University and Research (M.I.U.R.) Flagship InterOmics Project (cod. PB05).

References

[1] A. Albanese, L. Cheng, M. Ursino, N.W. Chbat, An integrated mathematical model of the human cardiopulmonary system: model development, Am. J. Physiol.-Heart C 310 (2015) H899–H921.
[2] A. Athanasiades, F. Ghorbel, J.W. Clark Jr., S.C. Niranjan, J. Olansen, J.B. Zwischenberger, A. Bidani, Energy analysis of a nonlinear model of the normal human lung, J. Biol. Systems 8 (2) (2000) 115–139.
[3] G. Avanzolini, P. Barbini, F. Bernardi, G. Cevenini, G. Gnudi, Role of the mechanical properties of tracheobronchial airways in determining the respiratory resistance time course, Ann. Biomed. Eng. 29 (2001) 575–586.
[4] J. Bai, L. Hongli, J. Zhang, B. Zhao, X. Zhou, Optimization and mechanism of step-leap respiration exercise in treating of cor pulmonale, Comput. Biol. Med. 28 (1998) 289–307.
[5] A.M. Bersani, E. Bersani, C. De Lazzari, Interaction between the respiratory and cardiovascular system: a simplified 0-D mathematical model, in: C. De Lazzari, M. Pirckhalava (Eds.), Cardiovascular and Pulmonary Artificial Organs: Educational Training Simulators, CNR Edizioni, Rome, 2017, pp. 87–103.
[6] E.J.M. Campbell, E. Agostini, J.N. Davis, The Respiratory Muscles: Mechanics and Neural Control, Lloyd-Luke, London, 1970.
[7] M. Capoccia, S. Marconi, S.A. Singh, D.M. Pisanelli, C. De Lazzari, Simulation as a preoperative planning approach in advanced heart failure patients. A retrospective clinical analysis, Biomed. Eng. Online 17 (1) (2018) 52, http://dx.doi.org/10.1186/s12938-018-0491-7.
[8] L.S. Costanzo, Physiology, second ed., WB Saunders Co, Phyladelphia, 2002.
[9] C. De Lazzari, M. Capoccia, S. Marconi, How can LVAD support influence ventricular energetic parameters in advanced heart failure patients? A retrospective study, Comput. Methods Programs Biomed. 17 (2) (2018) 117–126.
[10] C. De Lazzari, I. Genuini, D.M. Pisanelli, A. D'Ambrosi, F. Fedele, Interactive simulator for e-learning environments: a teaching software for health care professionals, Biomed. Eng. Online 13 (172) (2014).
[11] C. De Lazzari, M. Pirckhalava, Simulation in medicine: Clinical teaching and learning, Cardiol. Intern. Med. XXI (14) (2015) 28-0.
[12] C. De Lazzari, D. Stalteri, CARDIOSIM© Cardiovascular Software Simulator, Department of Biomedical Science, National Research Council of Italy, 2011, https://cardiosim.dsb.cnr.it/.
[13] L. Ellwein Fix, J. Khoury, R.R. Moores Jr., L. Linkous, M. Brandes, H.J. Rozycki, Theoretical open-loop model of respiratory mechanics in the extremely preterm infant, PLoS One 13 (6) (2018) e019842.
[14] E. Farag, M. Argalious, J.E. Tetzlaff, D. Sharma (Eds.), Basic Sciences in Anesthesia, Springer International PublishingAG, Cham, Switzerland, ISBN: 978-3-319-62067-1, 2018.
[15] F. Gaudenzi, A.P. Avolio, 2013. Lumped parameter model of cardiovascular-respiratory interaction. In: 45th Annual International Conference of the IEEE EMBS, 3–7 July. Osaka, Japan.
[16] J.F. Golden, J.W. Clark Jr., P.M. Stevens, Mathematical modeling of pulmonary airway dynamics, IEEE Trans. Biomed. Eng. 20 (6) (1973) 3247–3263.
[17] D.C. Grinnan, J.D. Truwit, Clinical review: Respiratory mechanics in spontaneous and assisted ventilation, Crit. Care 9 (2005) 472–484.
[18] A.C. Guyton, J.E. Hall, Textbook of Medical Physiology, eleventh ed., Elsevier Saunders, Philadelphia, Pennsylvania, ISBN: 0-7216-0240-1, 2006.
[19] R.S. Harris, Pressure-volume curves of respiratory system, Respir. Care 50 (1) (2005) 78–99.
[20] K. Hemalatha, M. Manivannan, Cardiopulmonary model to study interaction hemodynamics in muller maneuver, Int. J. Numer. Methods Biomed. Eng. 27 (2011) 1524–1544.
[21] K. Hemalatha, L. Suganthi, M. Manivannan, Hybrid cardiopulmonary model for analysis of Valsalva maneuver with radial artery pulse, Ann. Biomed. Eng. 38 (10) (2010) 3151–3161.
[22] F. Huang, Z. Gou, Y. Fu, X. Ruan, Effect on the pulmonary hemodynamics and gas exchange with a speed modulated right ventricular assist rotary blood pump: a numerical study, Biomed. Eng. Online 17 (142) (2018).
[23] A.C. Jackson, J.T. Milhorn Jr., Digital computer simulation of respiratory mechanics, Comput. Biomed. Res. 6 (1973) 27–56.
[24] R. Kardin, Understanding Pulmonary Pathology, Academic Press, ISBN: 9780128013045, 2016.
[25] V. Le Rolle, N. Samson, J.P. Praud, A.I. Hernandez, Mathematical modeling of respiratory system mechanics in the newborn lamb, Acta Biotheor. 91 (1) (2013) 91–107.

[26] C.H. Liu, S.C. Niranjan, J.W. Clark Jr., K.Y. San, J.B. Zwischehberger, A. Bidani, et al., Airway mechanics, gas exchange, and blood flow in a nonlinear model of the normal human lung, J. Appl. Physiol. 84 (1998) 1447–1469.
[27] K. Lu, J.W. Clark, F.H. Ghorbel, D.L. Ware, A. Bidani, A human cardiopulmonary system model applied to the analysis of the Valsalva maneuver, Am. J. Physiol.-Heart C 281 (2001) H2661–H2679.
[28] U. Lucangelo, P. Pelosi, W.A. Zin, Respiratory System and Artificial Ventilation, Springer-Verlag, Milan, Italy, ISBN: 978-88-470-0765-9, 2008.
[29] S. Marconi, C. De Lazzari, 2018. A lumped parameter model of airway/lung mechanics. In: Affenzeller, Bruzzone, Jiménez, Longo, Merkuryev and Piera (Eds.), Proceedings of the 30TH European Modeling and Simulation Symposium, pp. 54–58. ISBN: 978-88-85741-03-4.
[30] F.N. Masana, Respiratory system model based on PSPICE, Int. J. Microelectron. Comput. Sci. 6 (3) (2015) 102–109.
[31] C.T. McCartney, M.N. Weis, G.L. Ruppel, R.P. Nayak, Residual volume and total lung capacity to assess reversibility in obstructive lung disease, Respir. Care 61 (11) (2016) 1505–1512.
[32] C. Ngo, R. Schlözer, T. Vollmer, S. Winter, B. Misgeld, S. Leonhardt, 2015. A simulative model approach of cardiopulmonary interaction. In: World Congress on Medical Physics and Biomedical Engineering, En Jaffray, Toronto, Canada.
[33] M.F. Olender, J.W. Clark Jr., P.M. Stevens, Analog computer simulation of maximum expiratory flow limitation, IEEE Trans. Biomed. Eng. 23 (6) (1976) 445–452.
[34] T.J. Pedley, R.C. Schroter, M.F. Sudlow, Energy losses and pressure drop in models of human airways, Respir. Physiol. 9 (1970) 371–386.
[35] T.J. Pedley, R.C. Schroter, M.F. Sudlow, The prediction of pressure drop and variation of resistance within the human bronchial airways, Respir. Physiol. 9 (1970) 387–405.
[36] F. Rohrer, Flow resistance in human air passages and the effect of irregular branching of the bronchial system on the respiratory process in various regions of the lungs, Arch. Gen. Physiol. 162 (1915) 225–299.
[37] The MathWorks, Inc, Simulink User's Guide, Natick, MA, 2018.
[38] N.C. Tsai, R.M. Lee, Interaction between cardiovascular system and respiration, Appl. Math. Model. 35 (2011) 5460–5469.
[39] J.B. West, Pulmonary Pathophysiology: The Essentials, Lippincott Williams & Wilkins, ISBN: 978-1-451-10713-5, 2012.
[40] D. Zander, C. Farver, Pulmonary Pathology, Elsevier, ISBN: 9780323393089, 2012.